Observation of Multimode Quantum Correlations in Fiber Optical Solitons

S. Spälter, N. Korolkova, F. König, A. Sizmann, and G. Leuchs
Lehrstuhl für Optik, Physikalisches Institut der Universität Erlangen Nürnberg, Staudtstrasse 7/B2, D-91058 Erlangen, Germany
(Received 20 March 1998)

Quantum correlations of photon numbers in different spectral components of ultrashort optical solitons have been observed experimentally. These correlations are crucial for the understanding and characterization of the internal quantum structure of soliton pulses and contribute significantly to soliton squeezing by spectral filtering. The accessible information on the nonclassical state of the correlated spectral components is discussed with the example of two modes. The method may be generalized to obtain a complete quantum description of a multimode field. [S0031-9007(98)06700-3]

PACS numbers: 42.50.Dv, 03.65.Bz, 42.65.Tg

The observation of amplitude squeezing by self-phase modulation and spectral filtering of picosecond [1] and femtosecond pulses [2,3] in optical fibers stimulated the study of the quantum properties of solitons. The state of a Fourier-limited light pulse may be constructed from Fock states [4] in analogy to a single field mode,

$$|\psi\rangle = \sum a_n |n\rangle , \tag{1}$$

where the expectation value of the photon number operator $\langle \hat{n} \rangle$ represents the number of the photons in the pulse. The information on the field state $|\psi\rangle$ can be obtained using one of the quantum state reconstruction methods [5]. Among them, the optical homodyne tomography (OHT) has proved to be a powerful tool to accomplish the full characterization of a variety of nonclassical states and the vacuum [6–8]. The application of OHT to pulsed squeezed light allowed for experimental reconstruction of the photon number distribution [7], the density matrix, and the Wigner function [6].

However, these tomographic experiments with optical pulses only yield the information on the statistics of the pulse as a whole. The same holds for the experiments on the generation of pulsed squeezed light using the Kerr effect [9,10]. There the noise variances were averaged over the spectral and temporal modes. Consequently, the quantum characteristics of the distinct frequency components and thus the internal quantum structure of the pulse were not accessible.

In order to account for the full multimode character of a pulsed field, the OHT technique might be applied to the individual spectral or temporal components by using a narrow local oscillator. However, in this case the information on phase relations within the pulse is lost.

The more general problem involves the consideration of the complex multimode structure of the pulse. In contrast to the single-mode case of Eq. (1), it requires the analysis of the quantum state of the multimode field which may be expanded in multimode Fock states $|\{n_k\}\rangle = \prod_k |n_k\rangle$:

$$|\Psi\rangle = \sum_{\{n_k\}} a_{\{n_k\}} |\{n_k\}\rangle . \tag{2}$$

It includes thus not only the quantum description of the distinct spectral modes, but also takes into account the entanglement between the frequency components. The methods using balanced homodyne detection were suggested to sample the joint density matrix of the two correlated spatial-temporal modes [11] and to measure the quantum correlations at different times in optical pulses [12,13]. This technique was adopted for the experimental observation of classical two-time photon-number correlations [14].

Spectral nonclassical correlations in an optical fiber were first discussed for the four different modes of cw radiation produced by pumping at two well-separated frequencies [15,16]. For nonclassical light of this type, referred to as two- and four-mode squeezed states, quadrature phase noise reduction is achieved for the combined modes as a consequence of quantum correlations, while each of the separate modes exhibits excess noise.

In squeezed fiber solitons the presence of intensity correlations provides a new aspect to the characterization of the internal quantum noise structure. So far, numerical studies of the quantum nonlinear Schrödinger equation [17] have provided a qualitative explanation of soliton amplitude squeezing experiments [1–3] by calculating the intensity variances of the individual components in the pulse spectrum. In this Letter we report on the first experimental observation of the quantum correlations between the various spectral components. The internal spectral correlation distribution within the pulse is recorded, demonstrating a new experimental method to characterize the quantum state of a multimode field.

The experimental setup (Fig. 1) consists of a source of optical soliton pulses, a silica optical fiber, a variable spectral filter, and a detector [2,3]. A mode locked chromium-YAG laser [18] produces bandwidth-limited 130-fs (FWHM) soliton pulses centered at 1.5 μm. The pulses are launched into a 2.7-m polarization preserving single-mode optical fiber (3M, FS-PM-7811) at a fundamental soliton energy of 54 pJ (the choice of parameters corresponds to the maximum achieved short fiber

 0031-9007/98/81(4)/786(4)$15.00

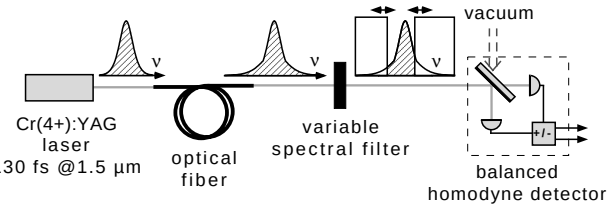

FIG. 1. Setup for the measurement of spectral intrapulse correlations.

squeezing by spectral filtering [3]). For all measurements described here both pulse energy and pulse width are kept constant to within 0.5%.

The fiber is followed by a variable spectral filter allowing for notch, high-, low-, or bandpass filtering [3]. The spectral resolution of the filter setup is 0.9 nm (90%/10% transmission points of the edge filter) which is considerably smaller than the spectral pulse width of 18 nm (FWHM). The transmitted light is measured using a balanced two-port detector [3]. The sum and difference rf noise currents from the two ports are recorded by two spectrum analyzers at a frequency of 20 MHz. The overall quantum efficiency of the setup is about 80% (including 93% grating efficiency, 6% overall losses at mirrors, lenses, and the beam splitter, and 92% detector quantum efficiency).

Measuring the classical mean field power spectra of the pulses (Fig. 2a), we find the output to be slightly Raman redshifted with respect to the input [19]. The output pulses are probed for internal two-mode correlations between two complementary frequency intervals within the pulse spectrum (Fig. 2b). By recording the noise current from both frequency intervals simultaneously (Fig. 2b, open circles) a coherent sum of all spectral noise components is detected. This measurement is accomplished with no filter applied, and the rms photocurrent noise is at the shot noise level as expected for light experiencing Kerr and Raman nonlinearities [20]. An incoherent sum is obtained by adding the two noise powers from the two individual intervals measured separately with the low-pass and the corresponding complementary high-pass filter for different cutoff wavelengths (Fig. 2b, full circles). We find that the incoherent sum generally is not at the shot noise level unlike the noise of unfiltered pulses. The difference is explained by the presence of correlations between the two complementary frequency intervals: the coherent sum detection corresponds to a superposition of the individual photon number variances Δn_i^2 $(i = 1, 2)$ from each of the two spectra and the covariance $\mathrm{cov}(n_i, n_j)$ between them

$$\Delta(n_1 + n_2)^2 = \Delta n_1^2 + \Delta n_2^2 + 2\,\mathrm{cov}(n_1, n_2)\,, \qquad (3)$$

with $\Delta n_i^2 = \langle \hat{n}_i^2 \rangle - \langle \hat{n}_i \rangle^2$ and $\mathrm{cov}(n_i, n_j) = \langle \hat{n}_i \hat{n}_j \rangle - \langle \hat{n}_i \rangle \langle \hat{n}_j \rangle$ $(i, j = 1, 2; i \neq j)$. In contrast, the incoherent detection corresponds to summing just the variances. Hence the covariance is a measure of the interference of

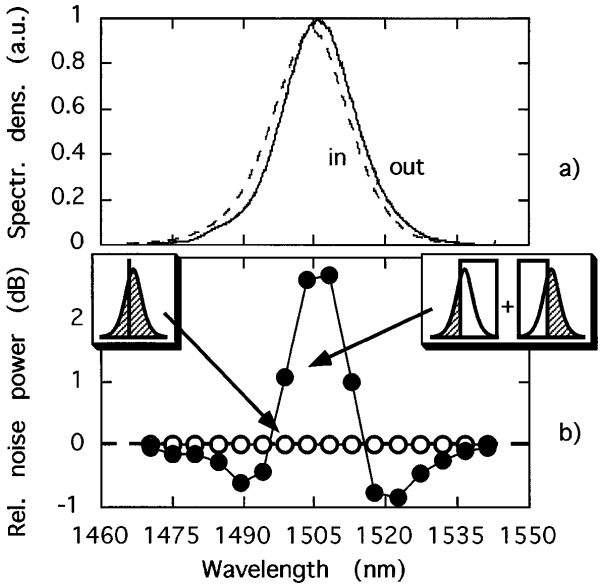

FIG. 2. In (a) the input and output spectra are displayed. In (b) the noise power detected simultaneously for all spectral components (open circles, left inset) is compared to the sum of the noise powers from complementary parts of the spectrum (full circles, right inset); all data are plotted relative to shot noise.

noise from the two spectra. The correlation coefficient $C(i, j)$ is defined as

$$C(i, j) = \frac{\mathrm{cov}(n_i, n_j)}{\sqrt{\Delta n_i^2\, \Delta n_j^2}}\,, \qquad (4)$$

where the normalization ensures $|C(i, j)| \leq 1$.

So far, the correlations were discussed for the long- and the complimentary short-wavelength side of the spectrum. For a more detailed description of the internal quantum noise structure the pulse output spectrum (Fig. 2a) was split into 15 wavelength intervals of equal width aiming at a measurement of correlations between arbitrary pairs. Hence, 15 variances of the individual intervals and 105 pair correlations had to be determined. This was achieved experimentally by adjusting the spectral filter such that wavelength windows $\{i_1, \ldots, i_m\}$ $(m \leq 15)$ were transmitted. Then, generalizing Eq. (3) the detected noise power reads as

$$\Delta\left(\sum_{i=i_1,\ldots,i_m} n_i\right)^2 = \sum_{i,j=i_1,\ldots,i_m} \mathrm{cov}(n_i, n_j)\,, \qquad (5)$$

where $\mathrm{cov}(n_i, n_i) = \Delta n_i^2$. For different filter configurations Eq. (5) forms a set of linear equations for the 120 unknown variances and covariances. 120 data points were recorded by varying systematically the width and the center position of a bandpass filter. Furthermore, a single interval notch filter was applied, contributing 13 additional data points. A standard method for solving this overdetermined set of linear equations yielded

the variances, the covariances, and the corresponding error bars.

Using Eq. (4), the correlation coefficients were calculated for $i \neq j$ and were plotted as off-diagonal elements in the matrix representation shown in Fig. 3. The x axis of the plot corresponds to wavelength component i, the y axis to wavelength component j, both relative to the center wavelength $\lambda_0^{\text{out}} = 1506$ nm. Each off-diagonal square in the plot represents the correlation of wavelength component i with wavelength component j. The correlation strength is encoded in the gray level: darker squares correspond to correlated, lighter squares to anticorrelated wavelength intervals. A second kind of information is provided in Fig. 3 for $i = j$: Instead of uninteresting correlation coefficients $C(i, i) = 1$ [Eq. (4)], the diagonal matrix elements represent the normalized difference between the measured variance Δn_i^2 and the measured shot noise $\Delta n_{i,sh}^2 = n_i$ for the corresponding wavelength interval

$$\tilde{C}(i, i) = 1 - \frac{n_i}{\Delta n_i^2}, \tag{6}$$

and thus give a measure of the internal correlation within one wavelength interval.

The correlation matrix (Fig. 3) has a characteristic butterfly pattern reflecting the internal quantum noise structure of the pulse. The asymmetry of the correlation pattern with respect to the center wavelength is due to the intrapulse Raman effect. Strong positive correlations are observed in the long-wavelength part of the spectrum. In its central part the frequency components are mainly negatively correlated. These intensity correlations between the individual pulse modes contribute significantly to noise reduction or enhancement. So far, squeezing by spectral filtering was attributed to sub-shot-noise variances of the individual frequency components [17]. The calculated variances [17] correspond to the diagonal matrix elements $\tilde{C}(i, i)$ of Eq. (6) which are all above shot noise for the experimental situation displayed in Fig. 3.

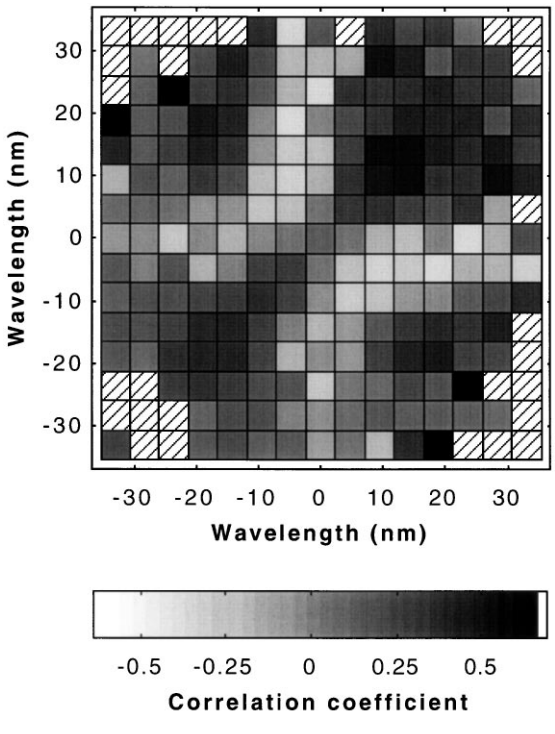

FIG. 3. Map of intrapulse quantum correlations. Each square represents the coefficient of correlation between the wavelength components as indicated on the axes of the diagram. The measured data points are displayed on one side of the diagonal and copied to the other side [$C(i, j) = C(j, i)$] for clarity. Correlation data in the outer low-intensity parts of the spectrum with a large error bar are represented by hatched squares.

Nevertheless, squeezing is observed due to the presence of internal correlations. Therefore the intrapulse quantum correlation structure mapped in Fig. 3 provides a clear insight into the mechanism of squeezing by spectral filtering. The noise reduction is obtained when the filter function is adjusted so that the negatively correlated parts of the spectrum are preserved while the positively correlated ones are cut off as much as possible. If no filter is applied, all correlation coefficients weighted by the corresponding variances [Eqs. (4) and (6)] must be summed, resulting in a signal at the shot noise level. For the diagonal elements one has to use $C(i, i) = 1$ in this case.

The Raman induced spectral asymmetry of the correlation matrix is in full agreement with the results of our earlier experiments [3]: significant squeezing was observed when a frequency high-pass filter was applied. It should be emphasized that the map of the intrapulse noise structure could generally serve as an efficient tool in optimizing squeezing, indicating which wavelength intervals have to be cut off in the process of spectral filtering.

The experiment may provide more information on the quantum state of the multimode field than can be displayed in the matrix of Fig. 3. To demonstrate this, the discussion is restricted to two wavelength components i and j of arbitrary widths ($i, j = 1, 2$). It is possible to characterize their correlation in a diagram, displaying the two-dimensional distribution of the probability to find n_i photons in channel i in coincidence with n_j photons in channel j. This probability distribution P_{ij} is given by the absolute squares $|a_{n_i n_j}|^2$ of the expansion coefficients in Eq. (2). This distribution may be determined experimentally by separately monitoring the two different channels and measuring the number of photons in coincidence.

The three independent variances measured in the experiment described above, Δn_1^2, Δn_2^2, and $\Delta(n_1 + n_2)^2$, are obtained when projecting the two-dimensional probability distribution $P_{12} = |a_{n_1 n_2}|^2$ onto the n_1 axis, the n_2 axis, and the diagonal, respectively (see Fig. 4b). Of course, these three numbers do not provide enough information to determine P_{12} in general. But if one assumes that the P_{12} distribution is a Gaussian shaped function, then its contour line is an ellipse. Its major and minor axes and the angle α_m between the major axis

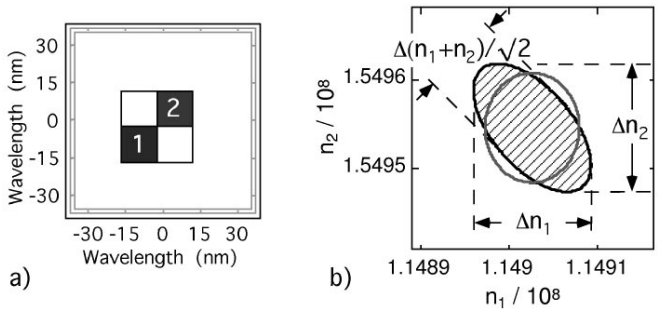

FIG. 4. (a) Measured correlation matrix and (b) quantum uncertainty (hatched ellipse) of two correlated modes. The open ellipse displays the two-mode shot noise contour. For the gray level in (a), see Fig. 3.

and the direction n_1 are uniquely determined by the three independent variances in the following way.

The photon number operator corresponding to the projection of P_{12} onto an arbitrary angle α and its variance are given by

$$\hat{N}(\alpha) = \hat{n}_1 \cos\alpha + \hat{n}_2 \sin\alpha\,, \tag{7}$$

and

$$\Delta N^2(\alpha) = \Delta n_1^2 \cos^2\alpha + \Delta n_2^2 \sin^2\alpha + 2\,\mathrm{cov}(n_1, n_2)\cos\alpha \sin\alpha\,. \tag{8}$$

The angle α_m is determined by $(\partial/\partial\alpha)\Delta N(\alpha)^2 = 0$. If $\mathrm{cov}(n_1, n_2) = 0$, then $\alpha_m = 0$. If $\Delta n_1^2 = \Delta n_2^2$, then $\alpha_m = \pm 45°$ where plus (minus) holds for $\mathrm{cov}(n_1, n_2)$ positive (negative). Otherwise

$$\tan(2\alpha_m) = \frac{2\,\mathrm{cov}(n_1, n_2)}{\Delta n_1^2 - \Delta n_2^2}\,. \tag{9}$$

To give an example, two particular wavelength intervals are chosen as indicated in Fig. 4a which uses the representation of Fig. 3. The corresponding correlation diagram is displayed in Fig. 4b. The hatched ellipse is reconstructed using the data of Fig. 4a. The open ellipse represents the contour line one would obtain if the correlation coefficient were zero and if the two wavelength components exhibited shot noise statistics. Figure 4b clearly shows that there is a projection ($\alpha \approx 45°$) for which the standard deviation $\Delta N(\alpha) = \sqrt{\Delta N^2(\alpha)}$ is below the shot noise level although the individual wavelength components are both above shot noise. It indicates the nonclassical character of this particular two-mode field.

As an alternative to measuring the correlation diagram directly as discussed above, it would also be possible to measure the projected probability distributions of $\hat{N}(\alpha)$ for arbitrary values of α and to process the data by standard tomographic methods [5].

In conclusion, we have demonstrated a method for reconstructing the spectral intensity uncertainties for arbitrary combinations of correlated modes and characterizing the corresponding photon number distributions. A complete characterization of a multimode quantum state must include the entanglement of different modes for arbitrary quadrature phase projections. Experimentally, the required wavelength selective phase shift may be achieved using an optical cavity [21,22].

It is a pleasure to acknowledge the help of G. Gardavsky with the data analysis. This work was supported by an EU grant under ESPRIT, No. 20029 (ACQUIRE). One of the authors (N. K.) gratefully acknowledges the support of the Alexander von Humboldt Foundation.

[1] S. R. Friberg, S. Machida, M. J. Werner, A. Levanon, and T. Mukai, Phys. Rev. Lett. **77**, 3775 (1996).
[2] S. Spälter, M. Burk, U. Strößner, M. Böhm, A. Sizmann, and G. Leuchs, Europhys. Lett. **38**, 335 (1997).
[3] S. Spälter, M. Burk, U. Strößner, A. Sizmann, and G. Leuchs, Opt. Expr. **2**, 77 (1998).
[4] F. X. Kärtner and L. Boivin, Phys. Rev. A **53**, 454 (1996).
[5] U. Leonhardt, *Measuring the Quantum State of Light* (Cambridge University Press, Cambridge, 1997).
[6] D. T. Smithey, M. Beck, M. G. Raymer, and A. Faridani, Phys. Rev. Lett. **70**, 1244 (1993).
[7] M. Munroe, D. Boggavarapu, M. E. Anderson, and M. G. Raymer, Phys. Rev. A **52**, R924 (1995).
[8] G. Breitenbach, S. Schiller, and J. Mlynek, Nature (London) **387**, 471 (1997).
[9] M. Rosenbluh and R. M. Shelby, Phys. Rev. Lett. **66**, 153 (1991).
[10] K. Bergman and H. A. Haus, Opt. Lett. **16**, 663 (1991).
[11] M. G. Raymer, D. F. McAlister, and U. Leonhardt, Phys. Rev. A **54**, 2397 (1996).
[12] T. Opatrný, D.-G. Welsch, and W. Vogel, Phys. Rev. A **55**, 1416 (1997).
[13] D. F. McAlister and M. G. Raymer, J. Mod. Opt. **44**, 2359 (1997).
[14] D. F. McAlister and M. G. Raymer, Phys. Rev. A **55**, R1609 (1997).
[15] B. L. Schumaker, S. H. Perlmutter, R. Shelby, and M. D. Levenson, Phys. Rev. Lett. **58**, 357 (1987).
[16] M. D. Levenson and R. M. Shelby, J. Mod. Opt. **34**, 775 (1987).
[17] M. J. Werner, Phys. Rev. A **54**, R2567 (1996); M. J. Werner and S. R. Friberg, Phys. Rev. Lett. **79**, 4143 (1997).
[18] S. Spälter, M. Böhm, M. Burk, B. Mikulla, R. Fluck, I. D. Jung, G. Zhang, U. Keller, A. Sizmann, and G. Leuchs, Appl. Phys. B **65**, 335 (1996).
[19] F. M. Mitschke and L. F. Mollenauer, Opt. Lett. **11**, 659 (1986).
[20] F. X. Kärtner, D. J. Dougherty, H. A. Haus, and E. P. Ippen, J. Opt. Soc. Am. B **11**, 1267 (1994).
[21] M. D. Levenson, R. M. Shelby, and S. H. Perlmutter, Opt. Lett. **10**, 514 (1985).
[22] J.-M. Courty, S. Spälter, F. König, A. Sizmann, and G. Leuchs, Phys. Rev. A (to be published).